

Seismic performance evaluation of a spring viscous damper cable system

Asad Naeem, Jinkoo Kim*

Department of Civil and Architectural Engineering, Sungkyunkwan University, Suwon, Republic of Korea

ARTICLE INFO

Keywords:

Seismic retrofit
Viscous dampers
Self-centering
Shaking table test

ABSTRACT

This research proposes a self-centering passive damping system consisting of a spring viscous damper linked with a preloaded tendon. The seismic performance of the spring viscous damper is evaluated by cyclic loading tests, and the results are used for the formulation of an analytical model of the retrofit system in the structural analysis program. The shaking table tests of a two-story steel frame installed with the proposed damping system are carried out using five different earthquake records. The results from the shaking table tests are verified by numerical simulation of the retrofitted structure. The results obtained from the experiments and numerical simulations demonstrate that the proposed damping system with added stiffness and self-centering capability is effective in reducing earthquake-induced displacement and member forces.

1. Introduction

The application of passive energy dissipation devices for the seismic protection of new and existing structures is increasing due to their ease of manufacturing, installing, and the introduction of suitable design guidelines. However even when passive dampers are applied for seismic protection, residual deformation in retrofitted structures may remain when subjected to severe ground motions. Residual deformations may result in complete loss of operational efficiency of the structure, and can significantly increase repair downtime and repair cost. To counter the drawbacks and enhance the performance of the passive damping devices, self-centering retrofitting systems have been extensively developed in recent years.

The seismic retrofit technique using dampers connected to pre-stressed cables was originally proposed by Pekcan et al. [1] as 'load-balancing pre-stressed tendon-fuse + damper (PTFD)'. The design procedure and installation criteria of the damped cable system were also presented in Ajrab et al. [2]. This technique was further developed using fluid viscous spring damper by Sorace and Terenzi [3]. Their study includes the dynamic experimental investigation of the damped cable system and an analytical case study on RC plane frame to determine the best performing cable layout and geometrical configuration. Choi et al. [4] also proposed a retrofitting technique of a viscoelastic damper with cables attached on the perimeter frame of a building.

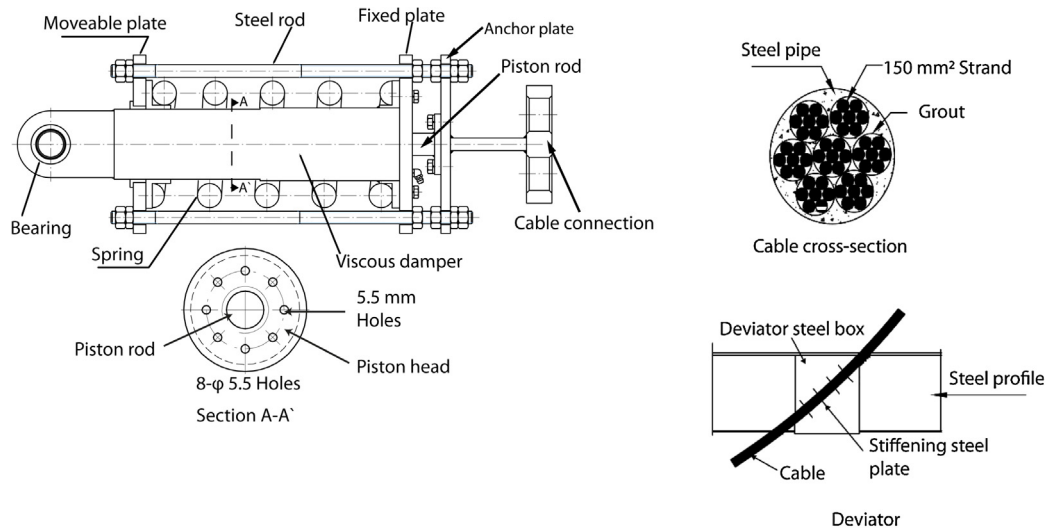
Self-centering retrofitting systems are a more suitable alternative to conventional passive dampers and stiffening of a structure. These self-centering systems can restore the structure back to its original position, hence eliminating or reducing the residual deformation in a

structure after an earthquake. The seismic performance of structures retrofitted with combined passive damping devices has been investigated in several studies. Tsai et al. [5] combined displacement-dependent and velocity-dependent devices and proposed an economical seismic retrofit solution. The seismic response of steel structures retrofitted with buckling-restrained brace in-series with viscoelastic dampers has been investigated by Marshall and Charney [6]. Bracing systems providing energy dissipation capacity and restoring force have been developed by Christopoulos et al. [7], Miller et al. [8] and Chou et al. [9]. Lee and Kim [10] and Lee et al. [11], developed a hybrid damping devices by combining steel slit and friction dampers connected in parallel and showed that the hybrid dampers are especially effective in reducing seismic responses for small to medium earthquakes, compared with slit or friction dampers with the same yield strength. The super-elastic property of shape memory alloy has been used to produce damping devices having both energy dissipation and self-centering capability [12,13]. Self-centering hybrid dampers using slit damper and shape memory alloy bars have been investigated by Naeem et al. [14].

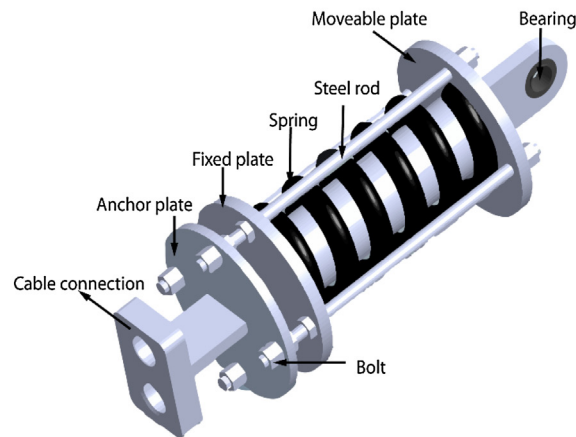
This study investigates the seismic performance of the spring viscous damper cable (SVDC) system, which consists of a viscous damper with external spring and a prestressed high strength steel cable. One end of the spring viscous damper is attached to the bottom of a structure, and the other end is connected to a pre-stressed steel cable which is fixed to an upper part of the structure. A silicon gel type viscous damper with an external spring is manufactured and is tested using a dynamic actuator to obtain its dynamic characteristics at different loading frequencies. An analytical model of the damper is developed using the parameters extracted from the test. Shaking table tests are

* Corresponding author.

E-mail address: jkim12@skku.edu (J. Kim).



(a) Sectional drawings



(b) 3-Dimensional illustration of damper

Fig. 1. Spring viscous damper.

carried out to investigate the seismic behavior of a 2-story steel structure retrofitted with the SVDC system. The test structure before and after the seismic retrofit is excited using five selected earthquake records scaled to a design spectrum and a maximum considered earthquake spectrum, and the retrofit effects of the SVDC are evaluated by comparing test results of the structure before and after the seismic retrofit. The results from the shaking table tests are validated by numerical analysis using the SAP2000 software, in order to further evaluate the efficiency of the proposed damping system.

2. Spring viscous dampers used in the experiment

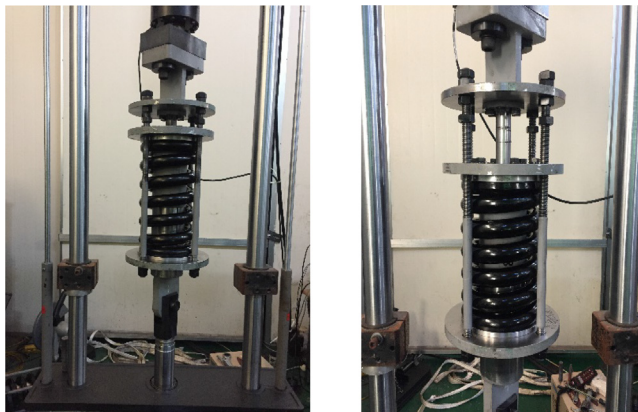
This section presents the results of cyclic loading tests performed on the full-scale prototype damper. The self-centering spring viscous damper is composed of a conventional viscous damper with an external heavy duty linear spring. The detailed schematicschematic drawings of the spring viscous damper, deviator zone, and cable cross-section are shown in Fig. 1(a). The spring is installed on the outer casing of the viscous damper as shown in the 3-dimensional illustration presented in Fig. 1(b). The spring is made of high tensile hard drawn steel or oil treated commercial steel which can provide the required spring stiffness for the damper. The spring is restrained between the ‘moveable plate’

and the ‘fixed plate’, while the viscous damper’s piston rod is rigidly connected to the ‘anchor plate’. The anchor plate is welded to an assembly which is used to connect the damper with the cable. The anchor plate and the fixed plate are connected to the steel rod, which can pass through the moveable plate. A viscous damping force is generated while silicone gel passes through orifices existing between the piston head and the vessel casing. A preload is applied on spring viscous damper during the installation of the SVDC system to a structure. Due to the preload applied to the cable during the installation process, the piston head of the viscous damper is moved to the center position and the spring is loaded in compression, which generates the recentering capacity of the device during earthquakes. This self-centering force is known to be effective in reducing earthquake-induced responses including residual deformation. The analytical expression for the damping and nonlinear elastic reaction forces of a spring viscous damper can be found in Pekcan et al. [15], Terenzi [16], and Sorace and Terenzi [17].

The prototype spring-viscous damper is manufactured to have the stroke of ± 50 mm with the spring stiffness of 1.2 kN/mm. The preload of 60 kN is applied to bring the damper to the neutral position, at which the spring is compressed to half of the full compression capacity. The prescribed loading protocol is presented in Table 1. The stroke of the

Table 1
Cyclic loading test protocol for spring viscous damper.

Test set	Velocity mm/s	Frequency Hz	Displacement mm	Total displacement mm	Force KN
1	15.7	0.5	2.5	5	63.3
2	31.4	0.5	5	10	66.4
3	47.1	0.5	7.5	15	73.8
4	62.8	0.5	10	20	78.3
5	78.5	0.5	12.5	25	81.1
6	94.2	0.5	15	30	83.6
1	31.4	1	5	10	66.2
2	62.8	1	10	20	79.6
3	94.2	1	15	30	85.0
4	125.6	1	20	40	90.2
5	157.0	1	25	50	95.0
6	188.4	1	30	60	100
1	39.3	2.5	2.5	5	63.7
2	78.5	2.5	5	10	70.6
3	117.8	2.5	7.5	15	78.3
4	157.0	2.5	10	20	81.3
5	196.3	2.5	12.5	25	84.2
6	235.5	2.5	15	30	88.9

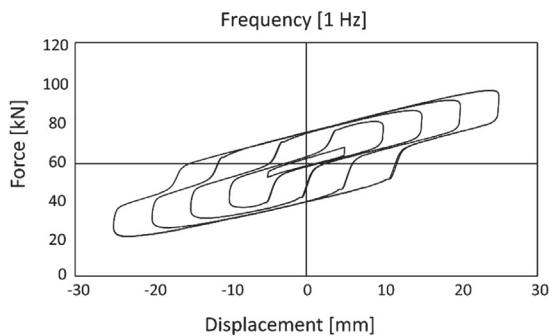


(a) Before preload (b) After preload

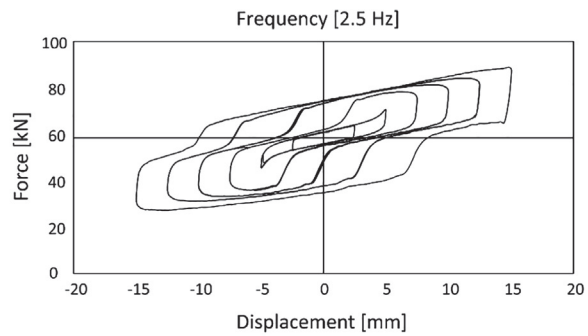
Fig. 2. Test setup for prototype spring viscous damper.

viscous damper is determined in such a way that the damper works without saturation at the maximum displacement of 1% of the story height.

Cyclic loading tests of the spring viscous damper are performed to understand the dynamic behavior of the damper including stiffness,



(a) Frequency=1 Hz



(b) Frequency=2.5 Hz

Fig. 3. Cyclic-loading test results of spring viscous damper at two different frequencies.

shape of hysteresis curve, frequency and displacement dependency, damping coefficient, velocity exponent, etc. The cyclic loading is applied starting from the neutral position. The tests are carried out in the frequency of 1.0 and 2.5 Hz with displacement varying from 5 to 30 mm. Each set of test is conducted in 10 cycles. Fig. 2 shows the spring viscous damper specimen vertically installed in the testing rig (100 kN UTM) before and after preload. The loading protocols and test results are presented in Table 1. Fig. 3 shows the force-displacement relationships of the test specimen at the loading frequency of 1 and 2.5 Hz. The forces at the maximum displacements appear to be symmetric both in tension and compression in all loading frequencies. The dissipated energy per cycle at the maximum stroke of ± 30 mm is computed to be 1,437.8 kN mm. Based on the test results, it is found that the prototype damper has damping coefficient of $C = 250 \text{ kN (s/m)}^\alpha$ and the velocity exponent (α) is 0.5.

The spring viscous damper is analytically modeled using the Maxwell model combined with other link elements connected in parallel as shown in Fig. 4. The dashpot link provides the damping while the multi-linear elastic link accounts for the stiffness of the spring viscous damper. The hook and gap elements are used for avoiding any spurious numerical response of the damper, and for stopping the device when the maximum stroke is reached in both tension and compression. The two stiffness coefficients for the bi-linear force-displacement relationships are determined from the experimental results. Further details on the mechanical behavior and the experimental and the analytical characteristics of the system can be found in [15–18]. The force displacement relationship of the spring viscous damper obtained at a frequency of 1 Hz is shown in Fig. 5 in comparison with the numerical simulation result, which demonstrates that the damper behavior can be accurately predicted with the analytical model within the test range.

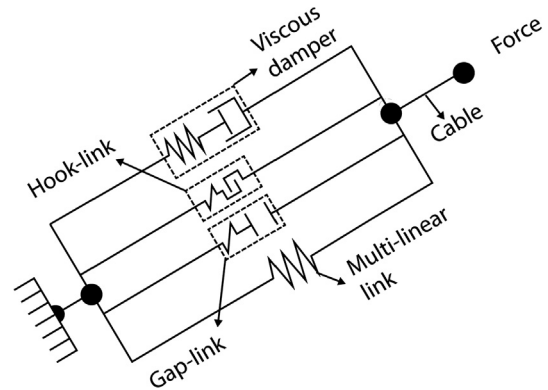


Fig. 4. Analysis model of the spring viscous damper.

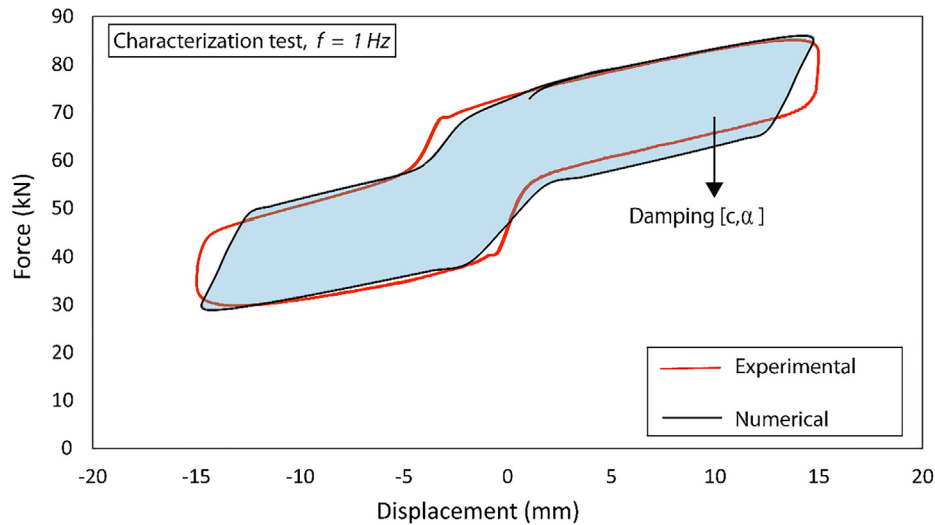


Fig. 5. Hysteresis curves of the prototype spring viscous damper obtained from the test and the analysis model.

3. Shaking table test setup

Preliminary design procedure of the SVDC system has been introduced in previous papers [1,3] including the determination of cross-sectional area of cable, stiffness of internal spring, the prestressing force of cable, etc. Generally the design is first carried out by determining the target fundamental period of the retrofitted structure necessary to reduce the maximum story drift within a target value. The maximum stroke of the spring viscous damper is determined according to the maximum acceptable drift of the structure required by the design code. In this study the SVDC system is designed in such a way that the fundamental natural period of the test structure decreases about 33% and the stiffness increases about 30% after the seismic retrofit. The retrofit system is installed in the longitudinal (x) direction of the mock up steel structure for the dynamic shaking table test. A pair of SVDC system are installed on both sides of the test specimen, and the structure is tested before and after the retrofit subjected to six ground motions scaled to

the design spectrum and three ground motions scaled to the maximum considered earthquake spectrum.

3.1. Test structure and instrumentation

The test specimen is a 2-story single bay steel structure consisting of

Table 2
Specifications of test structure.

Length (mm)	3675
Width (mm)	2850
Height (mm)	6000
Weight (Kgf)	12,000
Steel sections	Beams: 300 × 150 × 6.5 × 9 Columns: 300 × 175 × 7 × 11
Material	SS400 ($F_y = 235$ MPa, $F_u = 400$ MPa)
Elastic modulus	200 GPa

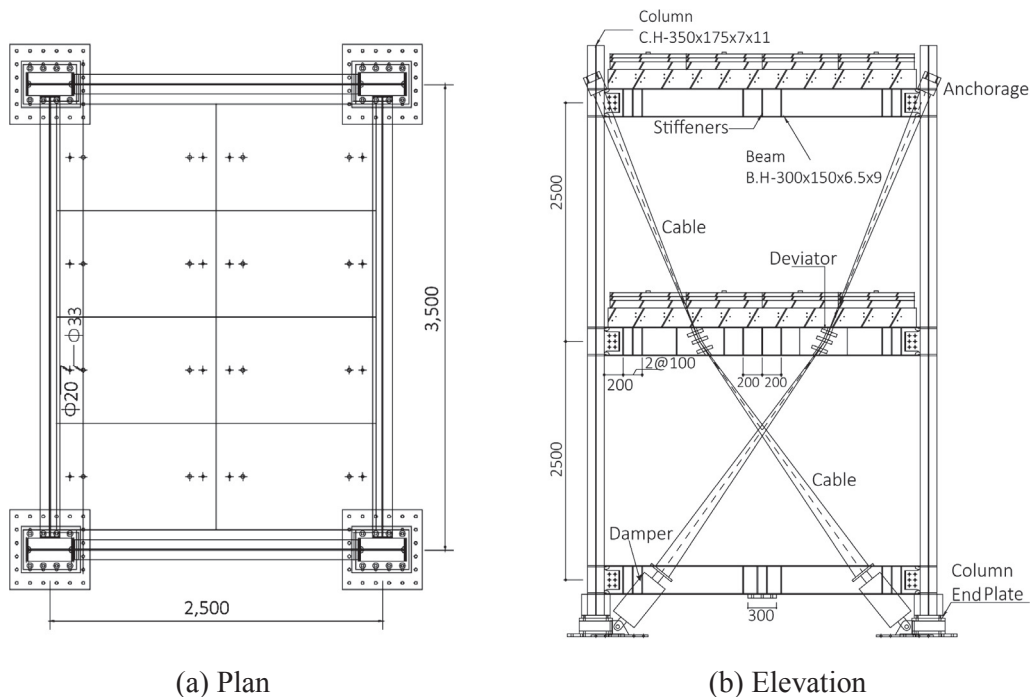


Fig. 6. Detailed drawing of the the test structure.

Table 3
Specifications of the shaking table used in the tests.

Items	Specifications
Maximum load	30,000 kgf
Table size	4.0 m × 4.0 m
Control axes	3 DOF (translational 2 axes, Rotational 1 axes)
Maximum displacement	± 300 mm
Maximum velocity	1.5 m/s
Frequency range	0.1–60 Hz
Excitation Mechanism	Electro-hydraulic servo, 3 variable control
Control software	MTS 469 D
Simultaneous data acquisition	264 channels (sample rating = 512 Hz)

H-shaped (wide flange) sections and reinforced concrete slabs with a thickness of 250 mm having a double layer of steel net reinforcement. The plan and elevation of the test specimen structure are shown in Fig. 6. The specifications of the test structure are shown in Table. 2. To retrofit the test structure four spring viscous dampers are installed at the base of the shake table. The spring viscous dampers are connected with four pairs of cables and each cable is loaded with 60 kN of pre-tension load. The SVDC system is installed in only weak longitudinal direction.

The seismic shaking table enables real-time observation of seismic

responses of structures by reproducing seismic waves on test models secured on the table. The shaking table used in the seismic performance test is a bi-axial (3-degree of freedom) shaking table equipment of the MTS corporation. The specifications of the shaking table are shown in Table 3.

The seismic response of the test structure is monitored through a network of instrumentation including 5 accelerometers, 6 displacement transducers, and 8 strain gages. The locations of the sensors are depicted in Fig. 7(a), and the perspective view is shown in Fig. 7(b). Three accelerometers are attached to the beams of the frame and two are installed in the center of the slab on each story. An additional accelerometer is also used to measure the acceleration of the shake-table. Six displacement transducers are used to collect the directional response of test structure on each level. To obtain the forces in the steel columns during the excitation, the strain gauges are installed at the bottom of each column. Fig. 8 shows the spring viscous damper and the cable/deviator after the installation of the SVDC system on the test structure.

3.2. Input ground motions

The input ground motions used for the shaking table tests, a white noise motion and five earthquake records, are applied in the horizontal direction. The ground motion records are scaled in such a way that the spectral acceleration of each record corresponding to the natural period of the structure matches with the target spectrum of Design Basis

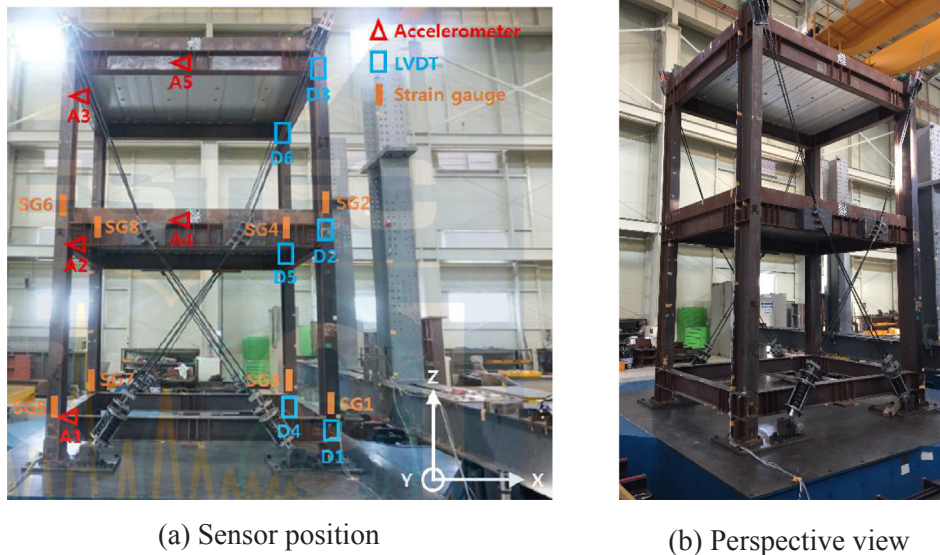


Fig. 7. Configuration of the test structure installed with SVDC system.

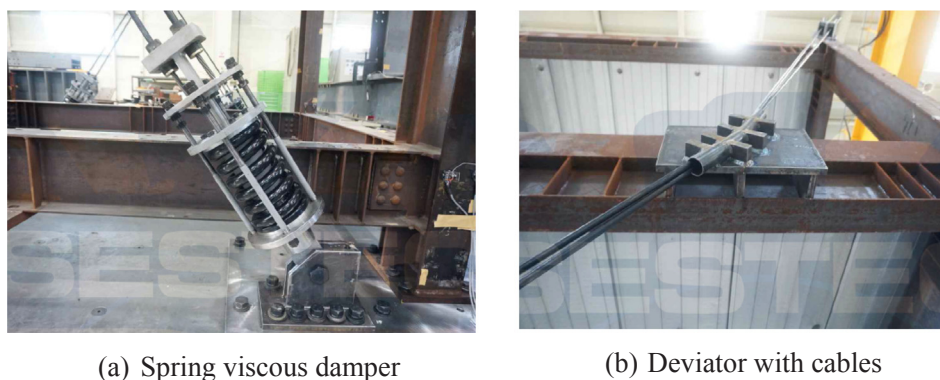


Fig. 8. SVDC system installation details.

Table 4
Earthquake records used for shaking table tests.

Case	Scaled level	Test No.	RSN	Earthquake name	Station name	Year	PGA (g)	Scale factor	Scaled PGA (g)	
Case 1 Retrofitted test structure specimen	#	1	Resonance search test 1: Random wave, amp = RMS 0.11 g, (0.5 Hz–50 Hz)							
		DBE	2	6	Imperial valley-02	El Centro	1940	0.28	0.69	0.19
			3	68	San FerenandoFernando	Hollywood	1971	0.23	0.81	0.184
			4	172	Imperial valley-06	El Centro	1979	0.14	1.74	0.241
			5	953	Northridge	Beverly Hills	1994	0.44	0.40	0.177
			6	1111	Kobe-Japan	Nishi Akashi	1995	0.49	0.36	0.175
	#	8	Resonance search test 2: Random wave, amp = RMS 0.11 g, (0.5 Hz–50 Hz)							
	MCE	9	6	Imperial valley-02	El Centro	1940	0.28	0.92	0.260	
			10	172	Imperial valley-06	El Centro	1979	0.14	2.20	0.310
			11	Resonance search test 3: Random wave, amp = RMS 0.11 g, (0.5 Hz–50 Hz)						
	Case 2 Original test structure specimen	#	12	Resonance search test 4: Random wave, amp = RMS 0.11 g, (0.5 Hz–50 Hz)						
DBE		13	6	Imperial valley-02	El Centro	1940	0.28	0.69	0.190	
			14	68	San FerenandoFernando	Hollywood	1971	0.23	0.81	0.184
			15	172	Imperial valley-06	El Centro	1979	0.14	1.74	0.241
			16	953	Northridge	Beverly Hills	1994	0.44	0.40	0.177
			17	1111	Kobe-Japan	Nishi Akashi	1995	0.49	0.36	0.175
#		18	Resonance search test 5: Random wave, amp = RMS 0.11 g, (0.5 Hz–50 Hz)							
MCE		19	6	Imperial valley-02	El Centro	1940	0.28	0.92	0.260	
			20	172	Imperial valley-06	El Centro	1979	0.14	2.20	0.310

Earthquakes (DBE) and Maximum Considered Earthquakes (MCE) in Seoul area. The spectral response accelerations at short period (S_{Ds}) and 1-second period (S_{D1}) are 0.497 g and 0.28 g, respectively, for the DBE level shaking. For the second set of ground motions, only two earthquake records and a white noise signal are scaled to the maximum considered earthquake (MCE) target spectrum ($S_{Ds} = 0.74$ g and $S_{D1} = 0.43$ g) to prevent possible collapse of the test specimen. The white noise signals are used to check any abnormality in instrumentation and to observe the change in natural frequencies of the test structure before and after the test. Table 4 shows the selected earthquake records used in the test, and Fig. 9 depicts the response spectra of the earthquake records scaled to the DBE and MCE response spectra.

4. Test results of the structure before and after seismic retrofit

Before running the test with each set of earthquakes, structural identification test is performed using white noise ground motions. The natural frequencies of the test structure are determined by calculating the transfer function of the response acceleration measured from the accelerometer (A5) positioned at the top of the roof slab relative to the input acceleration at the base of the shaking table. The transfer function is calculated by the cross power spectral density function of the input and output signals. The accuracy of the resonance analysis is improved by applying a symmetric hamming window to each input signal. The results of the resonance detection test for each case is shown in Table 5, and the estimated transfer function is shown in Fig. 10.

Figs. 11 and 12 show the displacement time histories of the test structure before and after the seismic retrofit subjected to the DBE and MCE level earthquakes, respectively. The displacement time histories depict the relative displacement of the roof displacement to the displacement of the base of the shaking table. They show the considerable reduction in the peak roof displacement of the retrofitted structure for both the DBE and MCE level earthquakes.

Fig. 13 compares the maximum roof displacement and acceleration of the test structure before and after installation of the SVDC system. It can be observed in Fig. 13(a) that the maximum displacement is reduced by from 68.5% in the case of DBE level El Centro (1940) to 48% in the case of El Centro (1979) earthquake after the retrofit. The comparison of the maximum acceleration of the test structure shows that the peak acceleration of the structure decreases in the retrofitted structure for most of the earthquake records, but slightly increases for the El Centro (1979) and Northridge ground motions scaled to the DBE. The maximum decrease of the roof acceleration is 38% for the San Fernando earthquake, and the maximum increase is 5.4% in the case of El Centro (1979) earthquake. The slight increase of the acceleration seems to be due to the fact that the stiffness provided by the prestressed

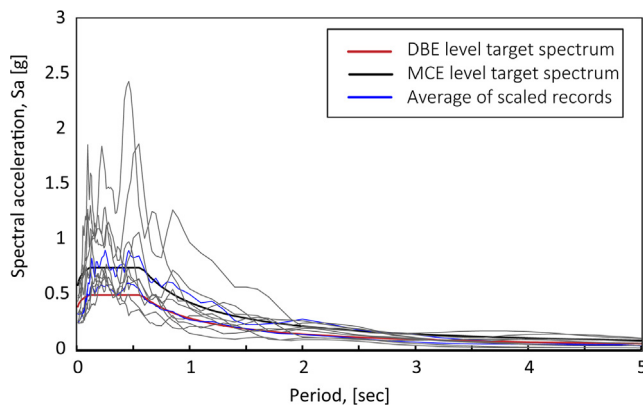


Fig. 9. Response spectra of the selected ground motions and the target spectra.

Table 5
White noise test results.

Resonance frequency (Hz), $f = 0.125$ Hz					
Case 1 (Retrofitted test structure)			Case 2 (Original test structure)		
Test no.	Orientation	Natural frequency (Hz)	Test no.	Orientation	Natural frequency (Hz)
1	Longitudinal (X)	4.625	12	Longitudinal (X)	2.875
8	Longitudinal (X)	4.750	18	Longitudinal (X)	2.875
11	Longitudinal (X)	4.250	–	–	–

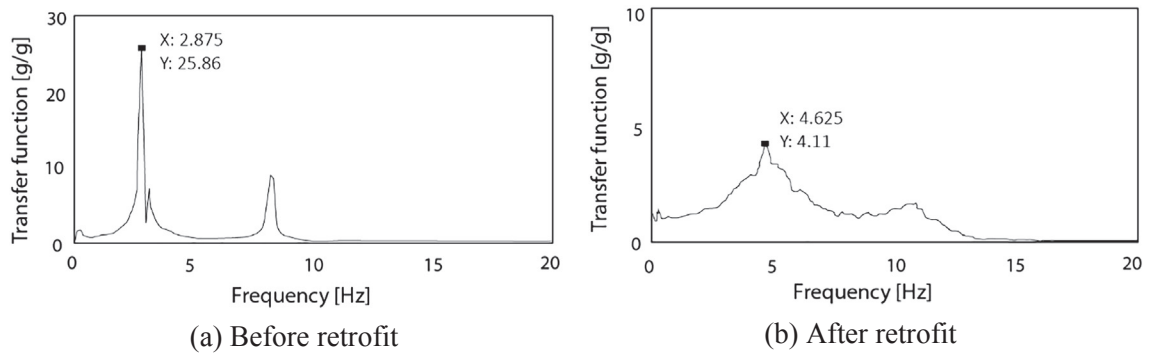


Fig. 10. Transfer functions of the test model before and after seismic retrofit.

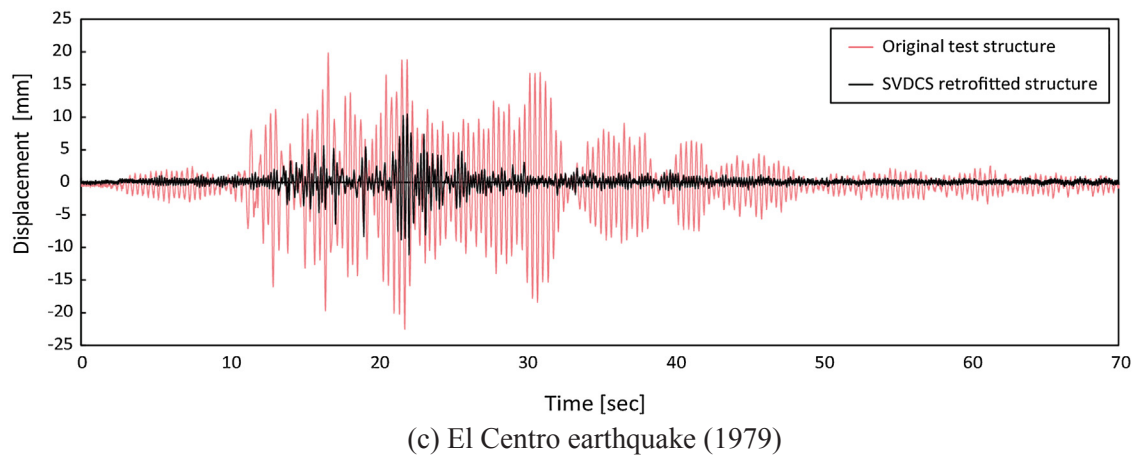
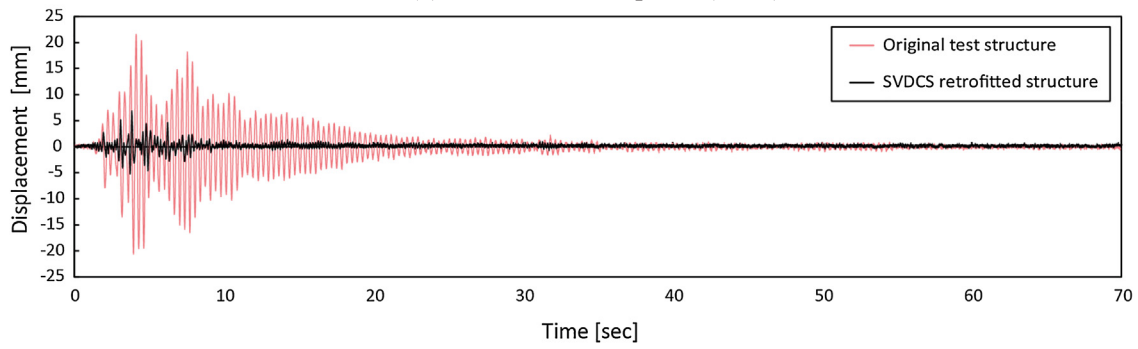
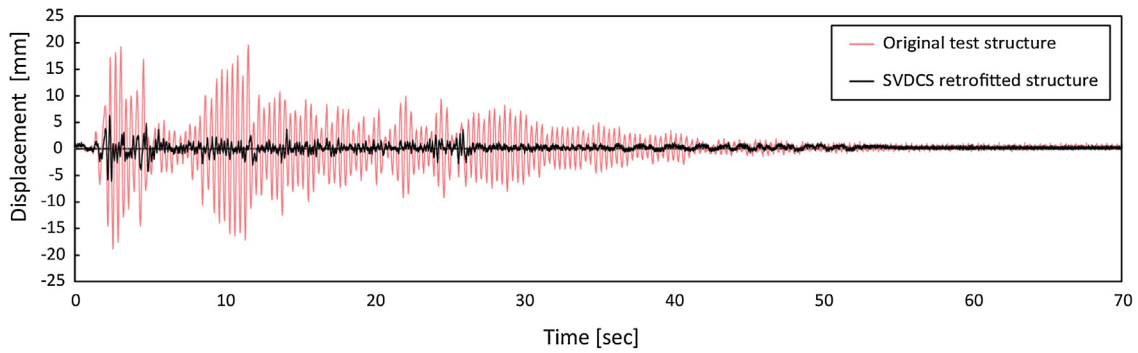
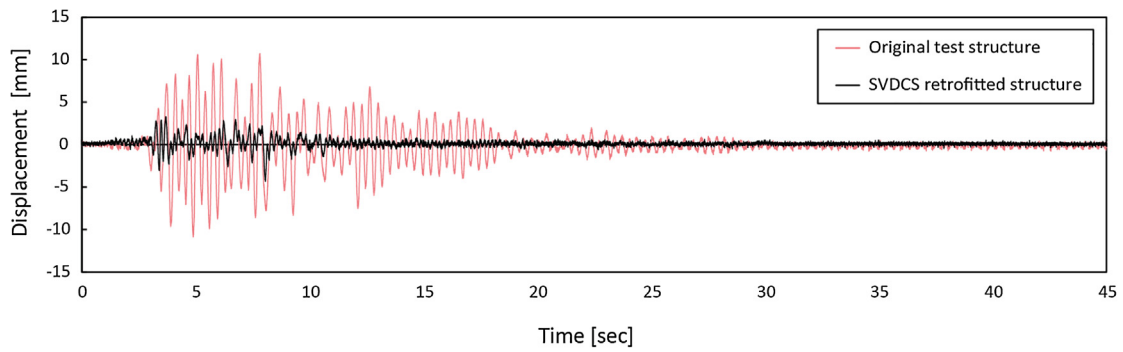
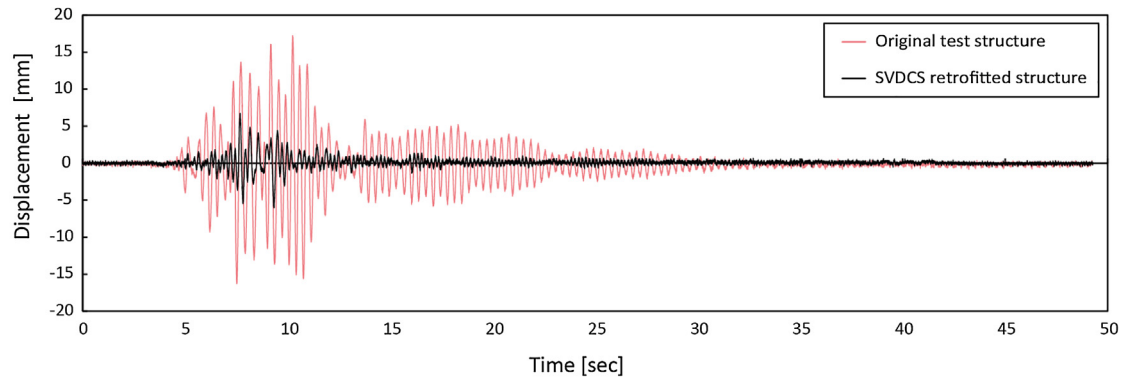


Fig. 11. Roof displacement time history of the test structure obtained from shaking table test for earthquake records scaled to DBE level.

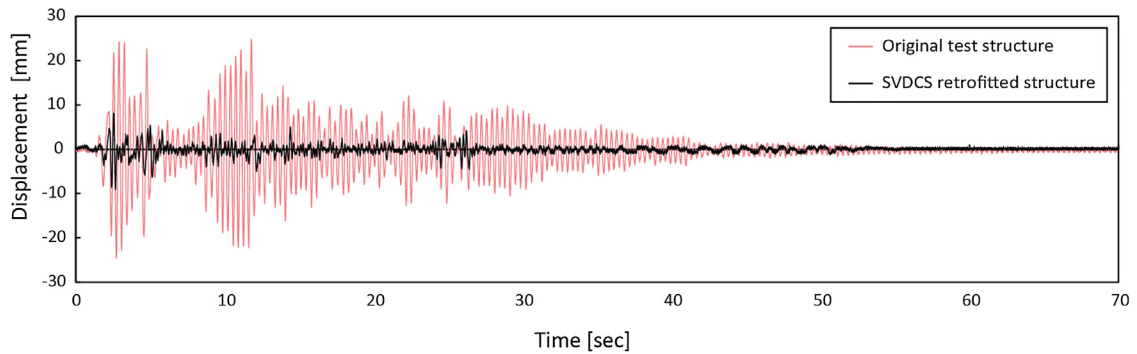


(d) Northridge earthquake (1994)

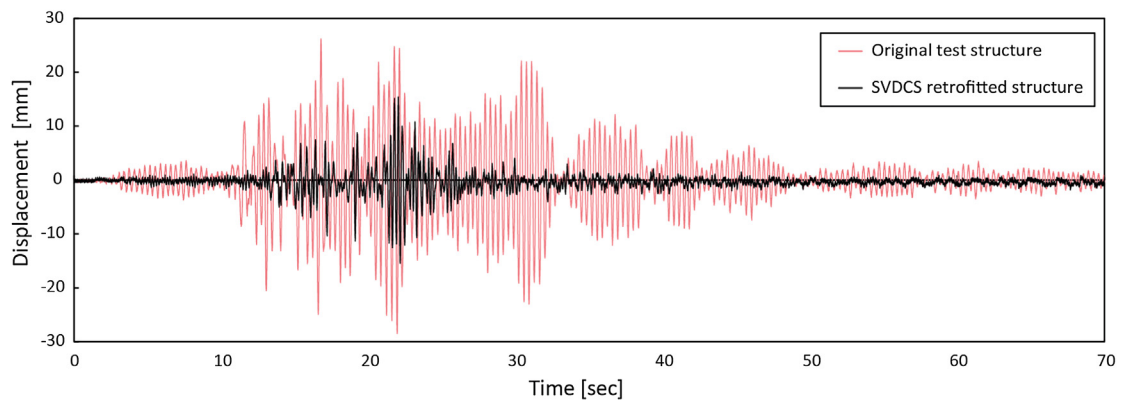


(e) Kobe earthquake (1995)

Fig. 11. (continued)

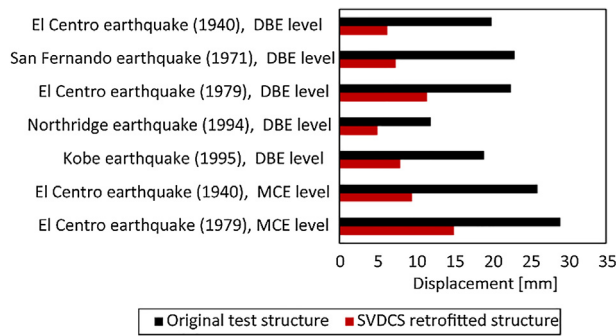


(a) El Centro earthquake (1940)

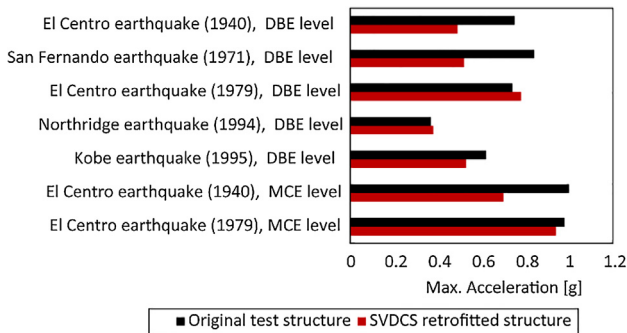


(b) El Centro earthquake (1979)

Fig. 12. Roof displacement time history of the test structure obtained from shaking table test for earthquake records scaled to MCE level.



(a) Maximum roof displacements

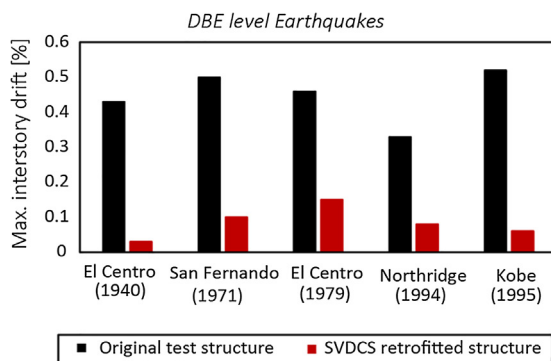


(b) Maximum roof accelerations

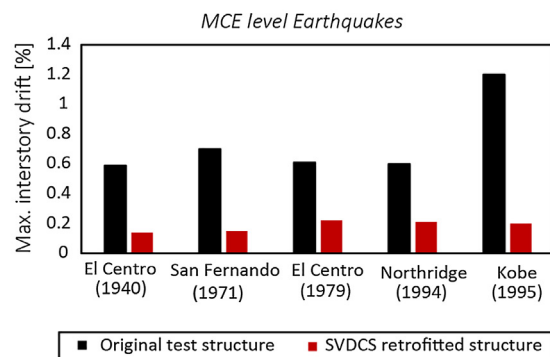
Fig. 13. Comparison of the response of the test structure before and after the seismic retrofit.

cables increases the natural frequency and consequently the seismic force induced by the ground motion. However, due to the participation of the viscous damping, the increase in the acceleration is only minute.

The maximum inter-story drifts of the test structure are presented in Fig. 14. The results for the Design Basis earthquakes are obtained from the tests, and those for the MCE excitations are from numerical analysis. The results show that with the application of the SVDC system the inter-story drift is reduced significantly both for the Design Basis earthquakes and the Maximum Considered earthquakes. More specifically, the reduction in the inter-story drift ranges from 89%



(a) DBE level earthquakes



(b) MCE level earthquakes

Fig. 14. Inter-story drifts of the original and retrofitted structure.

(El Centro, 1940) to 67% (El Centro, 1979) for Design Basis earthquakes, and 82% (Kobe earthquake) to 64% (El Centro, 1979) for Maximum Considered earthquakes.

The responses of the test structure obtained from the shaking table tests are compared with those obtained from the numerical analyses carried out using the SAP 2000 software in Figs. 15 and 16 to validate the accuracy of the analysis model. The spring viscous damper is modeled using the dashpot, hook, and multi-linear elastic link as discussed in Section 2. The inherent damping ratio of the structure is assumed to be 3% of the critical damping, which is modeled as Rayleigh damping. It can be observed that the agreement between the analysis and experimental results are generally satisfactory, especially in the region of strong motion duration.

Figs. 17 and 18 depict the time histories of shear and axial force of one of the first story columns, respectively, subjected to the design level El Centro 1940 and 1979 earthquakes obtained from the numerical analysis. The two records are selected because they are most effective (El Centro 1940) and least effective (El Centro 1979) in terms of acceleration response obtained from the test as shown in Fig. 14. It is observed that the column shear force reduces to 28% and 35% of those of the original structure after the retrofit, respectively. On the other hand, the reduction of column axial force is less effective; they reduce to only 77% and 83% of those of the original structure. Therefore the proposed retrofit system is effective in reducing displacement responses of a framed structure, but is not so effective in some responses such as floor acceleration and column axial force.

Fig. 19 represents the time histories of the absorbed energy in the test structure subjected to the MCE level Kobe earthquake obtained from numerical analysis. It is observed that before the seismic retrofit, 23% of the input seismic energy is dissipated by the inelastic deformation of the structural elements and the remaining energy is dissipated by the inherent modal damping. In comparison, in the retrofitted structure, up to 50% of the total dissipated energy is dissipated by the dampers and no energy is dissipated by the inelastic deformation of the beams and columns.

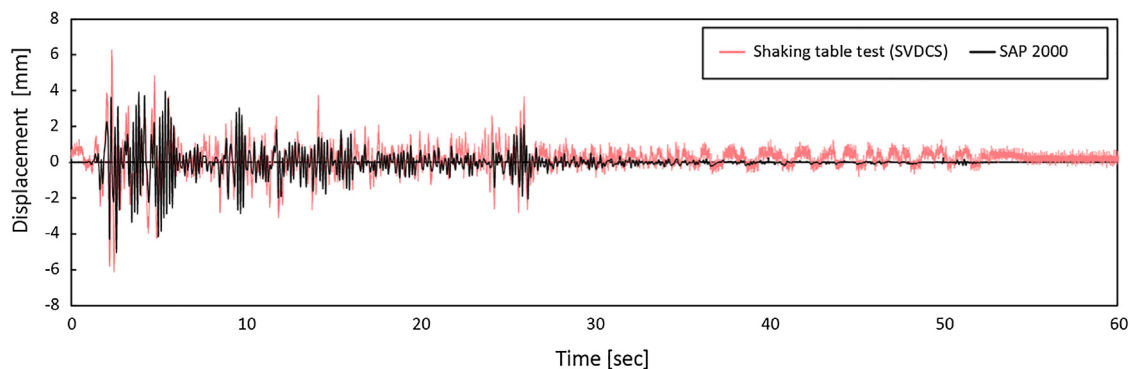
5. Conclusion

The aim of this study is to develop a self-centering seismic retrofit system consisting of a viscous damper with an external spring connected to a preloaded tendon and to investigate its seismic performance using shaking table tests. From the shaking table tests and numerical analysis of the model structure, the following observations were made:

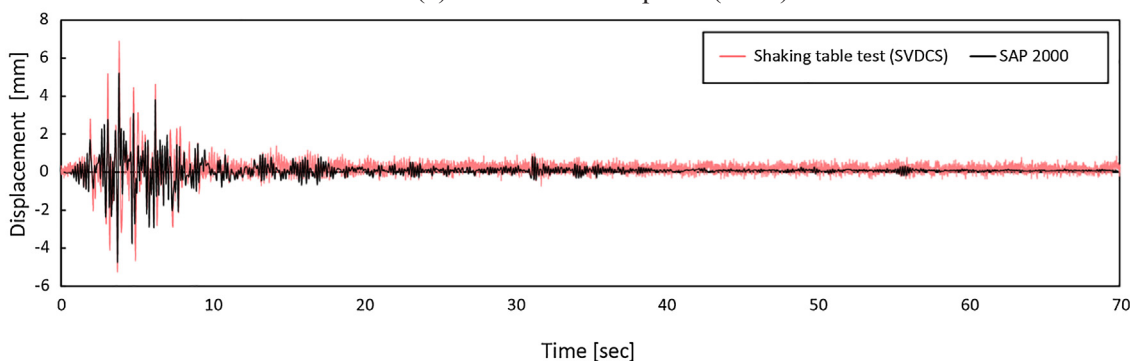
The proposed seismic retrofit system was effective in reducing

earthquake-induced roof and inter-story drifts, but not so effective in reducing floor accelerations and column axial forces. More specifically, the reduction in the maximum inter-story drift ranged from 89% (El Centro earthquake, 1940) to 67% (El Centro earthquake, 1979) for Design Basis earthquakes, and 82% (Kobe earthquake) to 64% (El Centro earthquake, 1979) for the Maximum Considered earthquakes. However the percentage reduction in the peak acceleration of the retrofitted structure was less than 40%, and for the El Centro (1979) and Northridge (1994) ground motions scaled to the DBE the roof acceleration in the retrofitted structure was slightly higher than that of the

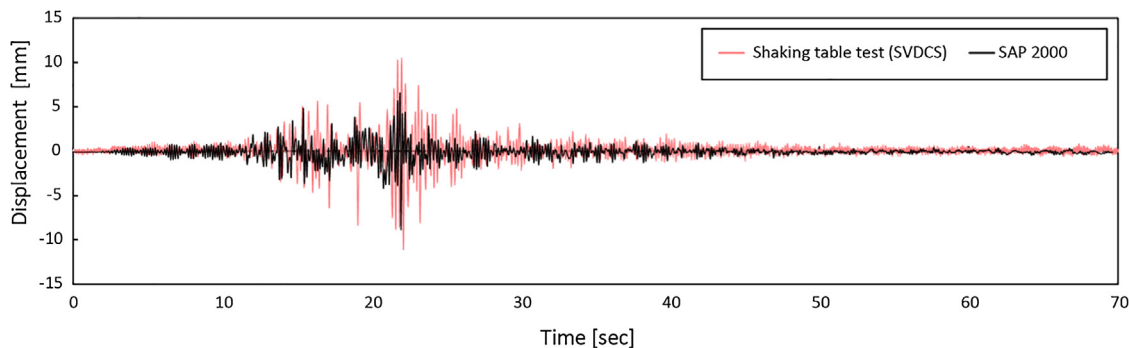
original test structure. According to the numerical analysis, the column shear force of the model structure subjected to the Design Basis El Centro 1940 and 1979 earthquakes was reduced to 28% and 35% of those of the original structure after the retrofit, respectively. On the other hand, the column axial force reduced to only 77% and 83% of those of the original structure. Based on the test and numerical analysis results, it was concluded that the spring viscous damper cable system with added stiffness, damping, and recentering force has a strong potential as an effective seismic retrofit technique of framed structures.



(a) El Centro earthquake (1940)

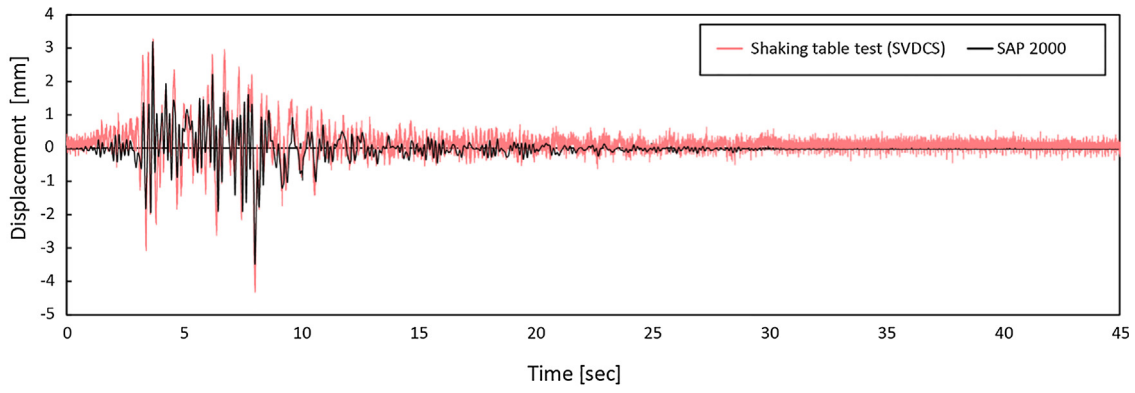


(b) San Fernando earthquake (1971)

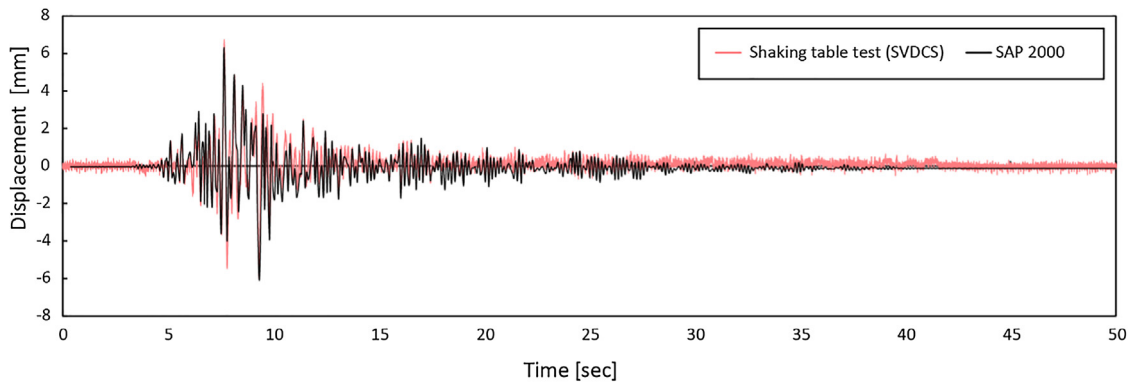


(c) El Centro earthquake (1979)

Fig. 15. Displacement time history of the retrofitted structure subjected to the design basis earthquakes obtained from shaking table test and SAP 2000 analysis.

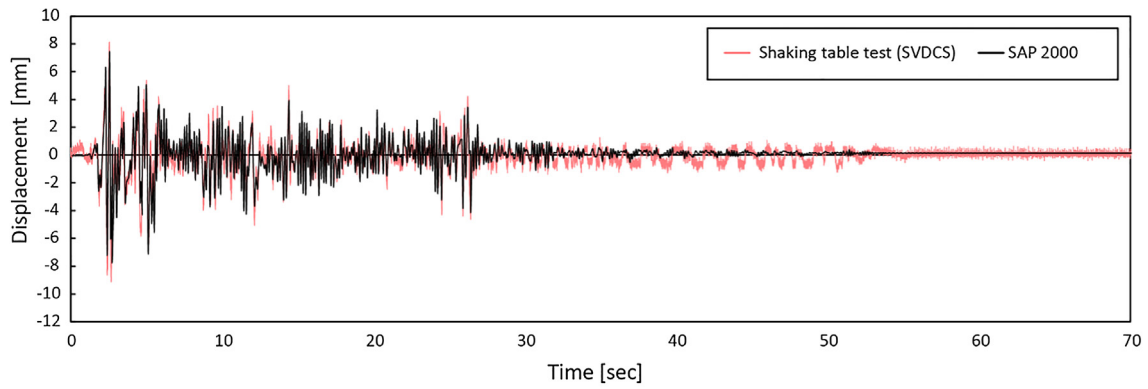


(d) Northridge earthquake (1994)

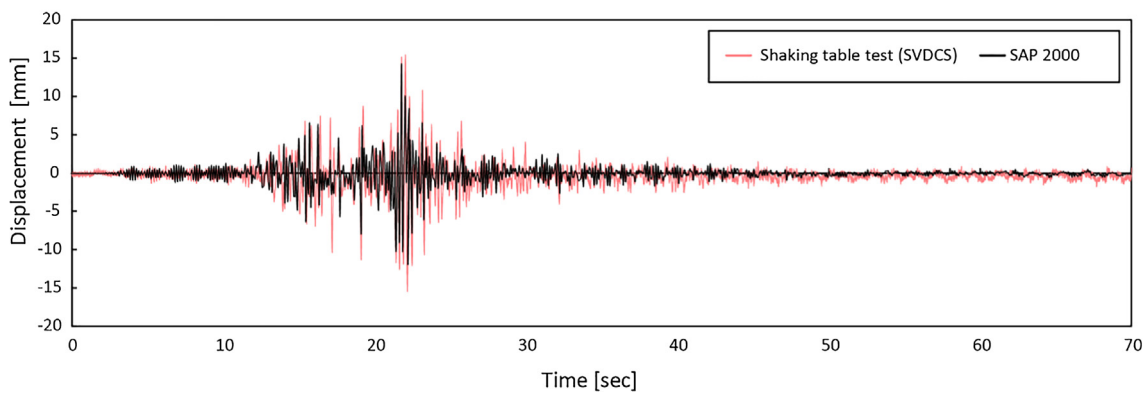


(e) Kobe earthquake (1995)

Fig. 15. (continued)



(a) El Centro earthquake (1940)



(b) El Centro earthquake (1979)

Fig. 16. Displacement time history of the retrofitted structure subjected to the maximum considered earthquakes obtained from shaking table test and SAP 2000 analysis.

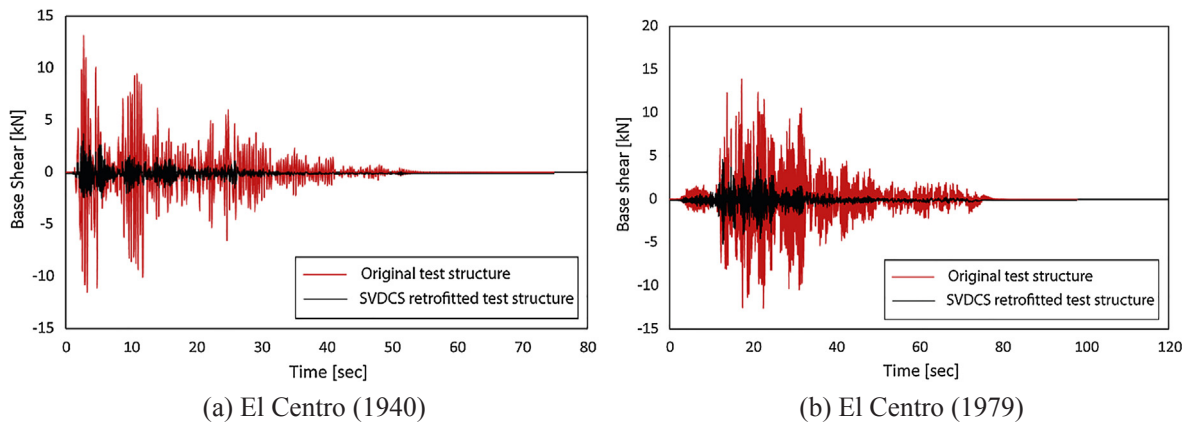


Fig. 17. Time history of the column shear force of the test structure without and with the retrofit.

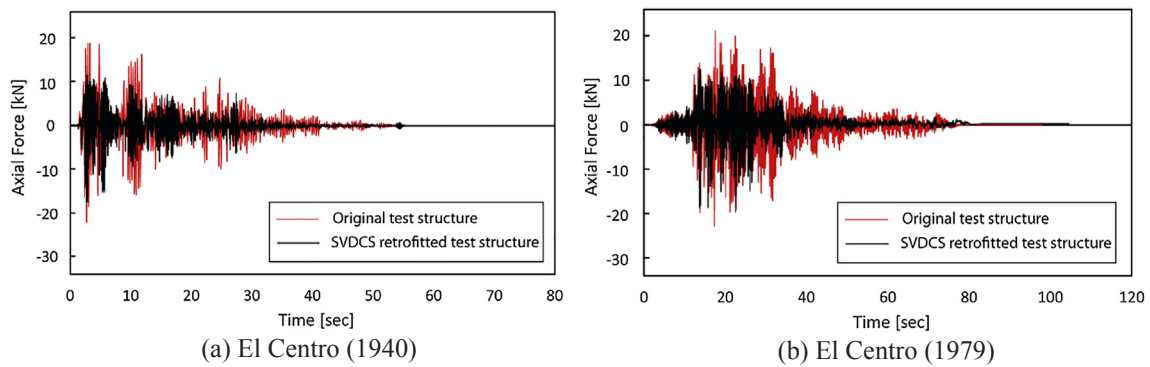


Fig. 18. Time history of the column axial force of the test structure without and with SVDCS.

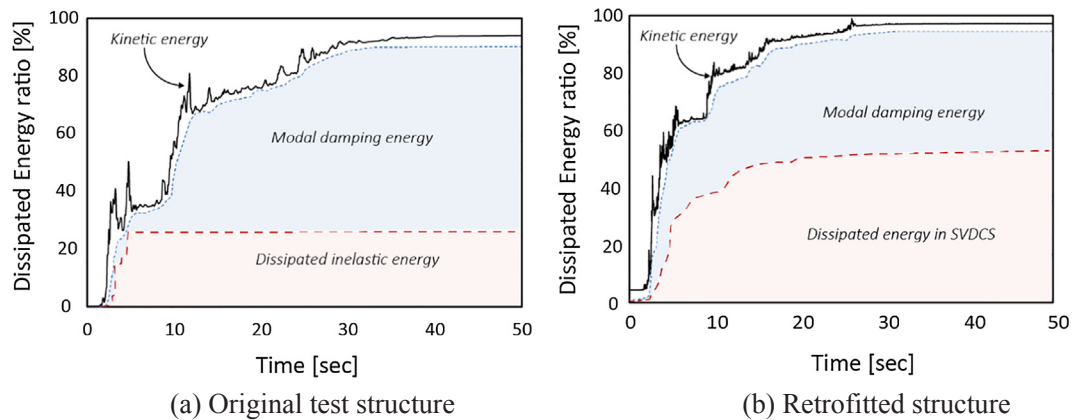


Fig. 19. Dissipated energy time history for Kobe earthquake.

Acknowledgement

This research was supported by a grant (code 17CTAP-C132889-01) from Technology Advancement Research Program (TARP) funded by Ministry of Land, Infrastructure and Transport of Korean government.

References

[1] Pekcan G, Mander JB, Chen SS. Balancing lateral loads using tendon-based supplemental damping system. *J Struct Eng* 2000;126(8):896–905.
 [2] Ajrab JJ, Pekcan G, Mander JB. Rocking wall–frame structures with supplemental tendon systems. *J Struct Eng* 2004;130(6):895–903.
 [3] Sorace S, Terenzi G. The damped cable system for seismic protection of frame

structures-Part II: design and application. *Earthq Eng Struct Dyn* 2012;41(5):929–47.
 [4] Choi H, Kim J. New installation scheme for viscoelastic dampers using cables. *Can J Civ Eng* 2010;37(9):1201–11.
 [5] Tsai CS, Chen KC, Chen CS. Seismic resistibility of high-rise buildings with combined velocity-dependent and velocity-independent devices. *ASME-Publications-PVP* 1998;366:103–10.
 [6] Marshall JD, Charney FA. Seismic response of steel frame structures with hybrid passive control systems. *Earthq Eng Struct Dyn* 2012;41(4):715–33.
 [7] Christopoulos C, Tremblay R, Kim HJ, Lacerte M. Self-centering energy dissipative bracing system for the seismic resistance of structures: development and validation. *J Struct Eng* 2008;134(1):96–107.
 [8] Miller DJ, Fahnestock LA, Eatherton MR. Development and experimental validation of a nickel–titanium shape memory alloy self-centering buckling-restrained brace. *Eng Struct* 2012;40:288–98.
 [9] Chou CC, Tsai WJ, Chung PT. Development and validation tests of a dual-core self-

- centering sandwiched buckling-restrained brace (SC-SBRB) for seismic resistance. *Eng Struct* 2016;121:30–41.
- [10] Lee J, Kim J. Seismic performance evaluation of moment frames with slit-friction hybrid dampers. *Earthq Struct* 2015;9(6):1291–311.
- [11] Lee J, Kang H, Kim J. Seismic performance of steel plate slit-friction hybrid dampers. *J Constr Steel Res* 2017;136:128–39.
- [12] Dolce M, Cardone D. Theoretical and experimental studies for the application of shape memory alloys in civil engineering. *J Eng Mater Technol* 2006;128(3):302–11.
- [13] Ingalkar Rameshwar S. Rehabilitation of Buildings and Bridges by Using Shape Memory Alloys (SMA). *Int J Civ Eng Res* 2014;5(2):163–8.
- [14] Naeem A, Eldin MN, Kim J. Seismic performance evaluation of a structure retrofitted using steel slit dampers with shape memory alloy bars. *Int J Steel Struct* 2017;17(4):1627–38.
- [15] Pekcan G, Mander JB, Chen SS. The seismic response of a 1: 3 scale model RC structure with elastomeric spring dampers. *Earthq Spect* 1995;11(2):249–67.
- [16] Terenzi G. Dynamics of SDOF systems with nonlinear viscous damping. *J Eng Mech* 1999;125(8):956–63.
- [17] Sorace S, Terenzi G. Non-linear dynamic modelling and design procedure of FV spring-dampers for base isolation. *Eng Struct* 2001;23(12):1556–67.
- [18] Sorace S, Terenzi G. Seismic protection of frame structures by fluid viscous damped braces. *J Struct Eng (ASCE)* 2008;134:45–55.